Solution Structure and Interactions of the *Escherichia coli* Cell Division Activator Protein CedA[†,‡]

Ho An Chen,[§] Peter Simpson,[§] Trevor Huyton,[§,||] David Roper,[⊥] and Stephen Matthews*[,§]

Department of Biological Sciences and Centre for Structural Biology, Imperial College of Science, Technology and Medicine, South Kensington, London SW7 2AZ, U.K., and Department of Biological Sciences, University of Warwick, Gibbet Hill Road, Coventry CV4 7AL, U.K.

Received January 5, 2005; Revised Manuscript Received March 23, 2005

ABSTRACT: CedA is a protein that is postulated to be involved in the regulation of cell division in *Escherichia coli* and related organisms; however, little biological data about its possible mode of action are available. Here we present a three-dimensional structure of this protein as determined by NMR spectroscopy. The protein is made up of four antiparallel β-strands, an α-helix, and a large unstructured stretch of residues at the N-terminus. It shows structural similarity to a family of DNA-binding proteins which interact with dsDNA via a three-stranded β-sheet, suggesting that CedA may be a DNA-binding protein. The putative binding surface of CedA is predominantly positively charged with a number of basic residues surrounding a groove largely dominated by aromatic residues. NMR chemical shift perturbations and gel-shift experiments performed with CedA confirm that the protein binds dsDNA, and its interaction is mediated primarily via the β-sheet.

Cell division is one of the most fundamental biological processes, and in bacteria, many of the proteins involved in this process have been identified and keenly studied (reviewed in refs *1*−*3*). Cell division requires the coordinated replication and segregation of the chromosome (*4*); however, the mechanisms responsible for the coordination between cell division and chromosome replication remain relatively ill-defined. A number of checkpoints for the control of cell cycle are present, whereby cell division may not proceed if initiation of replication is inhibited, segregation of chromosome is incomplete, or the DNA is damaged. Some of these checkpoints are poorly characterized on a molecular level, and there may be others that have yet to be discovered.

In *Escherichia coli* cells, the DnaA protein initiates the replication by binding to the bacterial replication origin (*oriC*). The replication is regulated by a number of mechanisms to ensure that only one replication occurs per cell division (*5*, *6*). For example, the newly synthesized strands are unmethylated during replication, and further replication is inhibited unless the new strands are methylated at GATC sequences by Dam methylase. However, for cells containing a cold-sensitive mutant of the DnaA protein, DnaAcos, the control of replication is defective (*7*) and the chromosome exhibits hyperactive initiation of replication, which results in the inhibition of cell division (*8*). Overexpression of CedA[1] in *dnaAcos* cells, however, is able to stimulate cell division without inhibiting the over-replication of the chromosome (*9*). This ability of CedA to suppress the *dnaAcos* mutant without inhibiting chromosomal over-initiation or over-replication implies a regulatory role for CedA involving an as yet unidentified pathway in the regulation of cell division, possibly a division inhibition pathway that serves as a checkpoint for the integrity of chromosomal replication during the cell cycle (*9*).

CedA is a small protein consisting of 87 residues, and homologues of this protein are found in other Gram-negative enterobacteria such as *Shigella flexneri* and *Salmonella typhimurium*. It has no homology with any other protein sequences of known structure. There is little information available on its precise role and how it may affect the stimulation of the cell division. Structural and biochemical characterization of this protein, however, may provide clues to the possible function of CedA via the study of the structural features of the protein and its structural homology to other proteins of known function. Such information will provide a basis for the design of future experiments that probe the role of CedA in cell division.

EXPERIMENTAL PROCEDURES

Expression and Purification of CedA. Uniformly ^{15}N- and ^{13}C-enriched protein of CedA was expressed for NMR analysis in minimal medium containing $^{15}NH_4Cl$ and [^{13}C]-

[†] The authors are indebted for the financial support of the Wellcome Trust and BBSRC. D.R. is grateful to the MRC for the career development award to T.H.

[‡] The atomic coordinates (PDB entry 2bn8) have been deposited in the Protein Data Bank.

* To whom correspondence should be addressed: Telephone: 44-(0)2075945315. Fax: 44(0)2075945315. E-mail: s.j.matthews@imperial.ac.uk.

[§] Imperial College of Science, Technology and Medicine.

[||] Present address: Walter and Eliza Hall Institute, Melbourne, Victoria 3050, Australia.

[⊥] University of Warwick.

[1] Abbreviations: CedA, cell division activator protein; NMR, nuclear magnetic resonance; NOE, nuclear Overhauser effect; TOCSY, total correlation spectroscopy; NOESY, nuclear Overhauser enhancement spectroscopy; rmsd, root-mean-square deviation; HSQC, homonuclear single-quantum coherence; PMSF, phenylmethanesulfonyl fluoride; Tris, tris(hydroxymethyl)amine; EDTA, ethylenediaminetetraacetic acid.

10.1021/bi0500269 CCC: $30.25
Published on Web 04/15/2005

D-glucose supplemented with vitamins; in this instance, 35 μg/mL kanamycin was used for the maintenance of the plasmid. The cells were lysed by sonication in 20 mM phosphate (pH 6.0); the clarified cell lysate was then initially purified on an SP-Sepharose ion exchange column. The column was washed with 20 mM phosphate buffer (pH 6.0) containing 100 mM NaCl, and the protein was eluted with a salt gradient. The fractions containing the protein were pooled, diluted four times, and further purified by being loaded onto a 5 mL Hi-trap heparin column (Pharmacia). The column was washed with 5 volumes of 20 mM phosphate buffer (pH 6.0), and the protein was eluted in stepwise fashion with 20 mL of phosphate buffers containing NaCl concentrations of 200, 300, and 500 mM. The protein was then dialyzed and concentrated in phosphate buffer. Some protein samples were truncated at the N-terminus after the SP ion exchange purification step by incubating the protein on ice for 2 h with 5 μL of 1 mg/mL trypsin. The trypsin digestion was terminated by the addition of PMSF, and the sample was then purified on the Hi-trap heparin column as before.

NMR Spectroscopy and Structural Calculation. NMR experiments were conducted on a 0.5 mM sample of CedA in 20 mM phosphate buffer (pH 3.8). The majority of NMR spectra were recorded at 303 K on a 500 MHz four-channel Bruker DRX500 spectrometer equipped with a z-shielded gradient triple-resonance cryoprobe. All chemical shifts were referenced using TSP [0 ppm (*10*)]. Backbone ^{1}H, ^{15}N, and ^{13}C resonances were assigned using the standard set of triple-resonance experiments, i.e., HNCO, HNCACB, and CBCA(CO)NH, with the H_α and H_β resonances assigned using HBHA(CBCACO)NH (for a review, see ref *11*). The assignment was then extended into the side chains using three-dimensional HCCH-TOCSY experiments (*12*), and the resonances of the aromatic side chains were assigned using a combination of ^{13}C,^{15}N-NOESY and (HB)CB(CGCD)HD spectra (*13*). All triple-resonance experiments employed constant-time evolution in the ^{15}N dimension, whereas in the CBCA(CO)NH and HBHA(CBCACO)NH experiments, both indirect dimensions were recorded in constant-time mode. The NMR spectra were processed and analyzed using NMRPipe (*14*) and XEASY (*15*), respectively.

A total of 360 long-range NOEs, providing unambiguous structural information, were manually assigned from the NOESY data. The ARIA protocol (*16*) was used for completion of the NOE assignment and structure calculation. A total of 1870 NOE-derived distances were assigned from ^{13}C- and ^{15}N-edited spectra, which comprised 1566 unambiguous and 304 ambiguous restraints. Dihedral angle restraints derived from TALOS were also implemented (*17*). The frequency window tolerance for assigning NOEs was $\pm$0.04 and $\pm$0.06 ppm for direct and indirect proton dimensions, respectively, and $\pm$0.7 ppm for nitrogen and carbon dimensions. The ARIA parameters, *p*, Tv, and Nv, were set to default values. The 15 lowest-energy structures had no NOE violations greater than 0.5 Å and dihedral angle violations greater than 5°. The structural statistics are presented in Table 1.

^{15}N T_1, ^{15}N T_2, and ^{1}H$-^{15}$N heteronuclear NOE data were measured on protein samples in 20 mM phosphate buffer (pH 3.8) using methods described previously (*18*, *19*). A single repeat was performed for two delays in each experiment, and these were used in evaluating uncertainties in peak intensity. Overlapped resonances were not included in the analysis.

Table 1: Structural Statistics for CedA Solution Structure Calculation

no. of experimental restraints	1966
total NOE-derived	1870
ambiguous	304
unambiguous	1566
intraresidue	806
sequential	277
medium-range ($\|i-j\| \leq 4$)	123
long-range ($\|i-j\| > 4$)	360
Talos (ϕ/ψ)	48
rmsd from experimental restraints	
distances (Å)	0.030 ± 0.002
dihedral angles (deg)	1.2 ± 0.3
rmsd from idealized covalent geometry	
bonds (Å)	0.0044 ± 0.00018
angles (deg)	0.57 ± 0.03
energy (kcal/mol)	
NOE	83.2 ± 25
bond	21.1 ± 1.8
angle	95.7 ± 10
vdw	-576 ± 10
coordinate rmsd (Å)	
backbone atoms in secondary structure	0.27 ± 0.07
heavy atoms in secondary structure	0.73 ± 0.1
Ramachandran plot[a]	
residues in most favored regions (%)	85
residues in allowed regions (%)	11
residues in disallowed regions (%)	4

[a] Structural quality was evaluated using PROCHECK_NMR (*37*).

DNA Binding Assays. The binding of CedA to dsDNA was assayed by band shift assays using 7.5% polyacrylamide gels buffered with 1× TBE. A 207 bp fragment of *Bacillus subtilis* GerE (J. Brannigan, personal communication) gene, amplified by PCR, was used as a nonspecific probe in these experiments. Assay mixtures were assembled containing 10 pmol of DNA with varying molar ratios of CedA protein as shown in Figure 5C in a total volume of 20 mL buffered with 20 mM Tris-HCl (pH 8.0), 5 mM $MgCl_2$, 0.5 mM $CaCl_2$, 0.1 mM EDTA, and 1 mM DTT. The reaction mixtures were incubated for 10 min at 37 °C prior to being loaded on the gel in a 40% glycerol, 0.25% bromophenol blue, and 0.25% xylene cyanol FF loading dye mixture. Electrophoresis was carried out at 40 V and room temperature for approximately 3 h prior to staining the gels with ethidium bromide for visualization.

For NMR mapping experiments, ^{15}N-labeled CedA samples were prepared in either 20 mM Tris-HCl buffer containing 250 mM NaCl or 20 mM phosphate (pH 7.2) at a protein concentration of approximately 30 μM in a volume of 0.5 mL. Purified and annealed dsDNA (CCGCGG or GCCGTTAACGCG) in the same buffer at ~1 mM was titrated into the CedA sample until a molar excess was achieved, and ^{15}N$-^{1}$H HSQC spectra were recorded at each stage under identical experimental conditions. Separate NMR binding experiments were conducted with both double-stranded samples (CCGCGG and GCCGTTAACGCG). Amide peak chemical shift changes were judged to be significant using a plot of $\Delta\delta(^{1}H)$ versus $\Delta\delta(^{15}N)$ as described previously (*20*) and were ranked using a weighted sum of the proton and nitrogen shift changes (*21*).

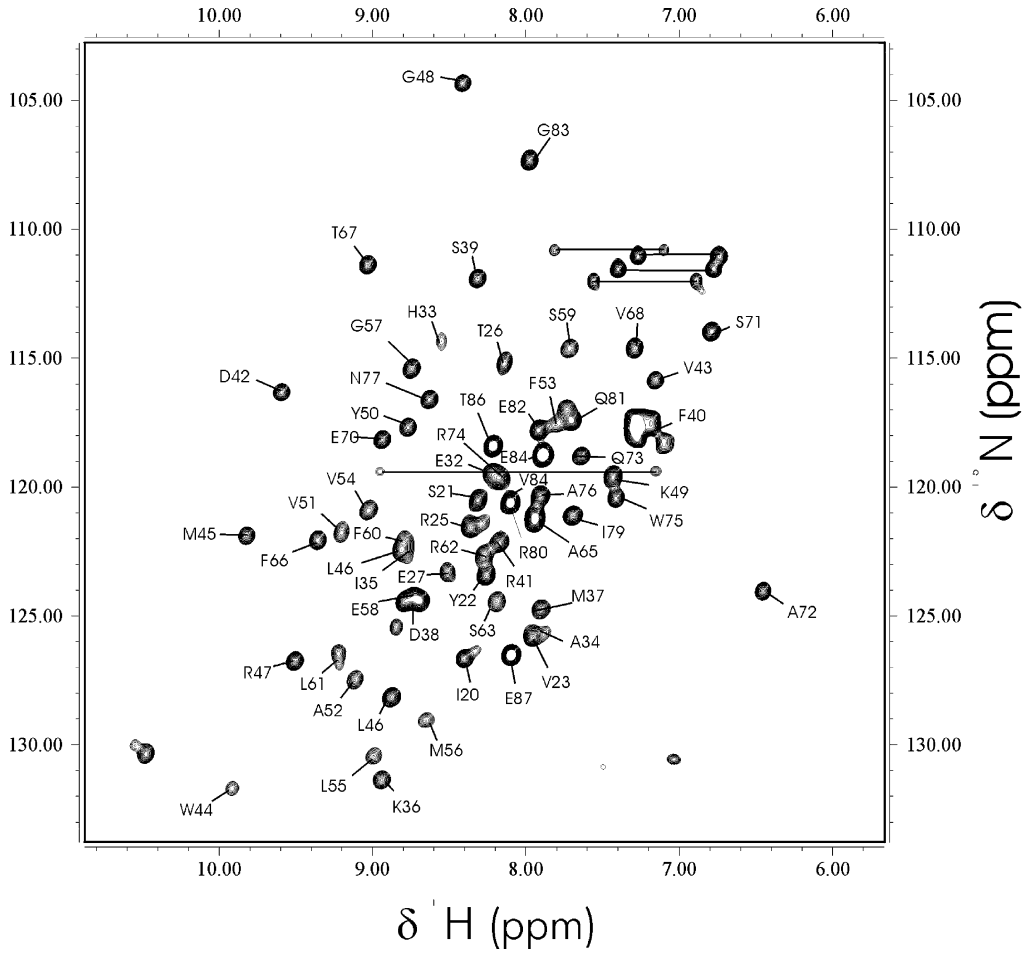

FIGURE 1: Assigned $^{1}H-^{15}N$ HSQC NMR spectra of the CedA truncated at the N-terminus. Side chain resonances for asparagine and glutamine residues are connected by horizontal lines. Sequential assignments of the backbone amides are shown.

RESULTS AND DISCUSSION

Solution Structure of CedA. The NMR assignment was initially performed on full-length CedA. Under alkaline conditions, the protein suffers from aggregation; therefore, all subsequent experiments were performed at pH 3.8. However, a large stretch of the N-terminus was assessed to be unstructured, and to resolve the ambiguities in the original assignments, subsequent assignment was performed on a truncated sample from which the first 17 residues had been removed. The chemical shifts of the residues in the truncated CedA are largely unchanged from those of the full-length protein, apart from a few residues immediately following the truncation site. An essentially complete assignment was obtained for the ^{1}H, ^{15}N, and ^{13}C resonances of the truncated protein, with the exception of a small number of resonances from the side chains of aromatic residues. Figure 1 shows the assigned HSQC spectrum for truncated CedA.

Using a combination of manual and ARIA NMR assignment methods for analysis of CedA (*16*), a total of 1870 nuclear Overhauser effects (NOEs) were assigned in CedA ^{15}N- and ^{13}C-edited NOESY spectra. The structure determination was also supplemented with 48 ϕ and φ dihedral angle restraints, amounting to an average of 24 restraints per residue. For the final iteration, the 15 lowest-energy structures were chosen from a total of 50 calculated on the basis of agreement with experimental data and structural quality (Table 1). All areas of secondary structure are very well defined (Figure 2A); the average pairwise rmsd for the water-refined final structures is 0.27 Å for the backbone atoms and 0.73 Å for the heavy atoms of residues within the secondary structure.

The structure of CedA showed a four-stranded antiparallel β-sheet and a C-terminal α-helix positioned almost parallel to the third strand (Figure 2B,C). The first 30 residues at the N-terminus exhibit increased flexibility with only a few NOEs observed for these residues. The first strand displays only limited characteristics of classical β-structure with only one pair of cross-strand hydrogen bonds between Lys35 and Met45, and runs antiparallel to the second (Val43−Leu46). Strand 2 is coupled to strand 3 (Lys49−Leu55) via a type I two-residue β-hairpin, while the hairpin loop between strands 3 and 4 (β34 loop) is less well defined within the NMR ensemble. The run of strand 4 is distorted by a proline (Pro64), creating a kink in the middle of the strand. This proline disrupts the normal pattern of cross-strand hydrogen bonds, and the side chain of Ser63 appears to act as a replacement for a backbone hydrogen bond that would otherwise be present. The C-terminal α-helix (Val68−Glu82) is packed along strand 3 via hydrophobic contacts from the side chains of Pro69, Ala72, Trp75, Ala76, and Ile79 to Tyr50, Ala52, and Val54 on strand 3, Val43 on strand 2, and Pro64 and Leu61 which lie on strand 4. This is further stabilized by a hydrogen bond network involving Asn77 and Arg80 on the helix andAsp42 and Arg41 on the loop at the

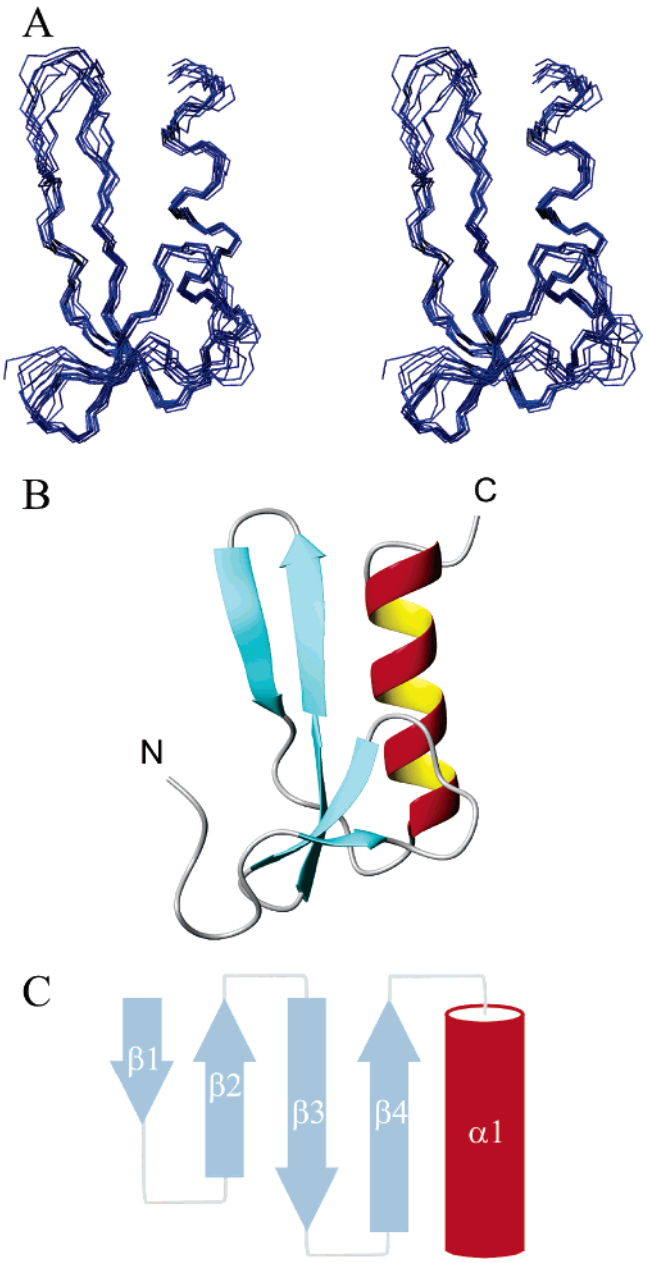

FIGURE 2: Solution structure of CedA. (A) Stereoview showing C_α traces representing the ensemble of NMR-derived structures. The 30 N-terminal amino acids are not shown for clarity. (B) Ribbon representation of a representative structure for CedA. All β-strands are colored blue, and the helix is colored red. The N-terminal amino acids are shown to illustrate their position relative to the β-sheet. (C) Topology diagram of the CedA structure.

beginning of strand 2. This hydrogen bond network may be responsible for unusually downfield shifted amide resonances observed for the side chain of Asn77.

To probe the dynamics of CedA, and in particular to examine the mobility of the β34 loop and the N-terminus, relaxation parameters (^{15}N T_1, ^{15}N T_2, and the steady-state heteronuclear ^{1}H−^{15}N NOE) were measured for ^{1}H−^{15}N backbone cross-peaks (Figure 3B−D). A full-length version of the protein was used for this analysis. High T_1 and T_2 values and low NOE values observed at the N- and C-termini reflect the increased flexibility in these regions and confirm the unstructured nature of the N-terminus. A significant degree of mobility is also observed on the pico- to nanosecond time scale in the β34 loop, which is reflected by the

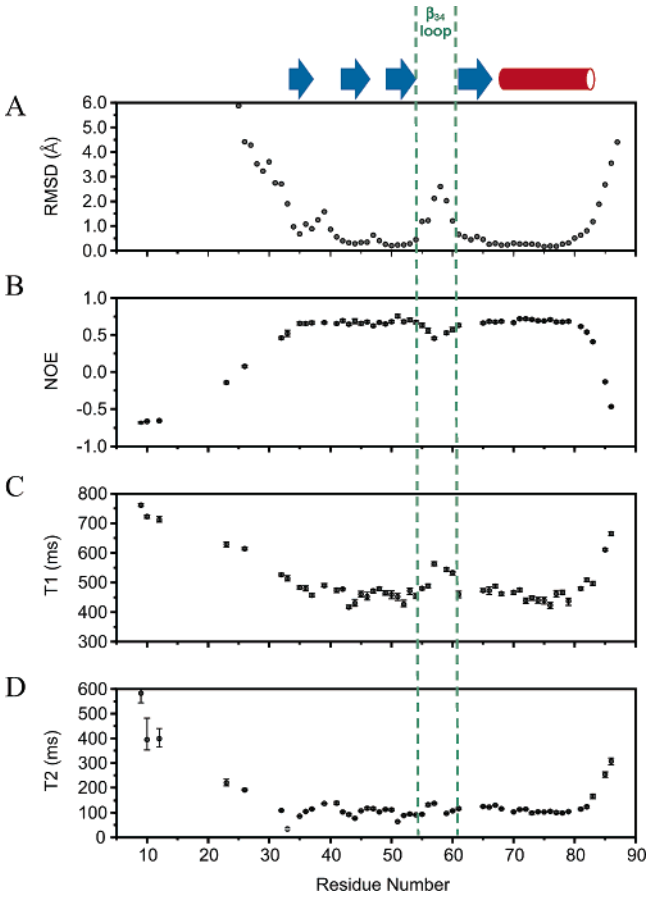

FIGURE 3: Sequence dependence of rmsd and ^{15}N relaxation data for CedA. (A) Sequence dependence of backbone coordinate position rmsd. (B) Sequence dependence of ^{1}H−^{15}N NOE values. (C) Sequence dependence of ^{15}N T_1 values. (D) Sequence dependence of ^{15}N T_2 values.

lower definition in this region within the NMR ensemble (see Figure 3A).

CedA Is Similar to dsDNA-Binding Domains. A search of the three-dimensional structure database with DALI (*22*) yielded two structures that resemble that of CedA: a GCC box binding domain (GBD) of ethylene-responsive transcription factor AtERF1 from *Arabidopsis thaliana* (*23*) and the N-terminal DNA-binding domain of λ-integrase protein (λ-INT-DBD) from bacteriophage λ (*24*) (shown in Figure 4). Both these proteins belong to a family of DNA-binding proteins that also includes the N-terminal DNA-binding domain of Tn*916* integrase (Tn*916*-DBD) (*25*). These proteins bind DNA with sequence specificity via the three-stranded β-sheet through the major groove of the DNA. CedA has no obvious sequence homology to these proteins but nevertheless shows striking structural similarities (Figure 4). With the exception of the presence of an extra short strand, CedA has structural elements similar to the elements of these proteins such as the longer pair of β-strands and the unusual arrangement of the α-helix which is packed almost parallel against the first of the longer pair of β-strands. The hydrogen bond network involving Asn77 between the helix and β-sheet echoes the hydrogen bond that exists between Asn52 and Asn15 of λ-INT-DBD. Furthermore, the proline that disrupts the edge β-strand in CedA also has its counterpart in λ-INT-DBD as a β-bulge (*26*).

The analogous binding surface of CedA is concave, which would be necessary to follow the curvature of dsDNA if the

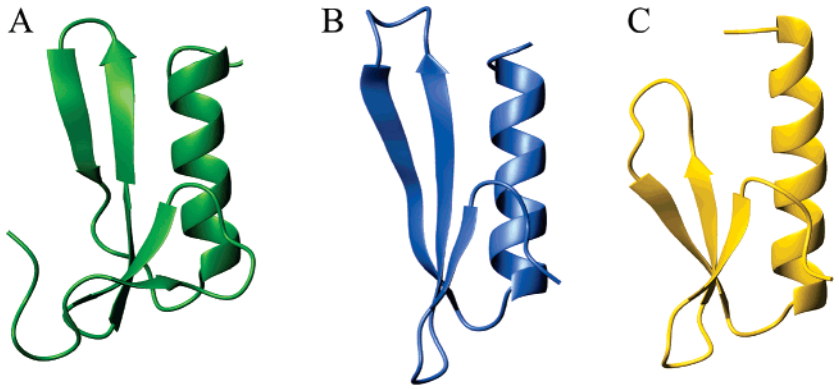

FIGURE 4: Structural comparison of CedA with GBD and λ-INT-DBD. (A) Ribbon representation of a representative structure for CedA. (B) Ribbon representation of a representative structure for GBD in the same orientation as panel A. (C) Ribbon representation of a representative structure for λ-INT-DBD in the same orientation as panel A.

β-sheet is to be situated within the major groove (Figure 5A). Previous studies have identified the residues that are important for recognition in this class of DNA-binding motifs (*24*, *27*). A number of positive charges (His33, Lys36, Arg41, Arg47, Lys49, and Arg62) encircle this putative binding surface, while the other side of the protein has only one positive charge but three negative charges (Figure 5B). The electrostatic map of CedA is thus consistent with the protein being able to bind DNA. Furthermore, the N-terminal domain of λ-INT-DBD has a 10-residue unstructured N-terminus that is rich in basic residues, and the presence of at least two consecutive positive charges in this unstructured region has been demonstrated to be necessary for efficient DNA binding (*24*). CedA has a much larger stretch of unstructured N-terminus, and it contains six basic residues within the first 20 residues. The major difference between CedA and these structures is the presence of the short, additional strand (β1).

CedA Interacts with dsDNA. The similarity of the structure of CedA to GBD, λ-INT-DBD, and Tn*916*-DBD suggests that dsDNA is a ligand for CedA. To test the hypothesis that CedA can bind dsDNA, we performed binding studies using a gel-shift assay. The retardation of the DNA in the presence of CedA indeed demonstrates that CedA has significant affinity for dsDNA (Figure 5C). NMR experiments involving analysis of amide line widths and chemical shifts were therefore performed for CedA in the presence of dsDNA to determine the nature of CedA's interaction with dsDNA. Several peaks in the HSQC spectrum broaden upon the addition of dsDNA, while other amide resonances move position, signifying an interaction and likely contact with the ligand (Figure 5D). Interestingly, a cluster of shifts occurs around the proposed binding surface on the β-sheet such as Ala52, Ala65, and Phe66, with the most significant being in the β34 loop (Val54, Ser59, and Phe60) (Figure 5F). Furthermore, there are additional residues experiencing shifts in the C-terminal end of the helix (Arg80, Gln81, and Gly83). Although many peaks within the N-terminal segment could not be assigned due to rapid solvent exchange of the amide proton and overlap, some peaks from the N-terminus such as Thr26 and Glu27 can be clearly seen to shift. Experiments repeated with distinct dsDNA sequences reveal the identical pattern of chemical shift movements. Furthermore, analysis of binding isotherms reveals an estimated dissociation constant for the CedA−dsDNA interaction of 103 ± 50 μM (Figure 5E), while no measurable interaction is observed for single-stranded alternatives.

DNA-Binding Mode of CedA. The similarity of CedA to the family of proteins which includes GBD, λ-INT-DBD, and Tn916-DBD suggests that it may also bind dsDNA by inserting the β-sheet into the major groove of the DNA. The putative binding surface of CedA is concave, but convex at the β34 loop, a feature which would permit the molecule to follow the curvature of the DNA helix while fitting into the major groove in the manner as observed in GBD (*23*). Previous studies have identified the residues that are important for DNA recognition in this class of three-stranded DNA-binding motifs (*24*, *27*, *28*). If CedA binds in the same manner, it may be expected that the backbone amide of Asp42 and the side chain of Lys49 of CedA will anchor the protein onto the phosphate groups on opposite strands of the DNA backbone, while residues such as Trp44, Arg47, and Arg62 may project into the groove and contact the bases for sequence-specific recognition. While no change in chemical shift is observed for the backbone of Asp42 upon addition of DNA, changes in chemical shift are observed for Arg47 and Lys49.

An interesting difference between CedA and three-stranded DNA-binding motifs is the presence of the extra β-strand (β1). The increased width of the β-sheet may preclude the entire β-sheet from being inserted into the major groove in the manner observed for the other domains. It is therefore possible that CedA may recognize dsDNA in a variation of the binding mode seen in GBD and DBD. A range of recognition modes exist for the binding of β-strand to dsDNA, from the use of a wide β-sheet to cover the minor groove in the family of TATA box-binding proteins (*29*) to the two-stranded major groove binding mode of MetJ repressors (*30*) and the five-stranded β-sheet arranged perpendicular to the DNA axis as seen in Glial cell missing (GCM) transcription factor domain (*31*). Of particular interest are the four-stranded β-sheet proteins that include the methyl-CpG binding domains from human methylation-dependent transcriptional repressor MBD1 (*32*) and MeCP2 (*33*). MBD1 may bind the major groove of the DNA and the phosphate backbone primarily via a flexible loop between strands 2 and 3, part of the α-helix, and its preceding loop. The flexible loop of MBD1 becomes ordered upon binding of the DNA, and the binding surface is relatively small when compared with those of the GBD and DBD family of proteins. The pattern of shift perturbations seen in CedA indicates that only strands 3 and 4 may be inserted into the

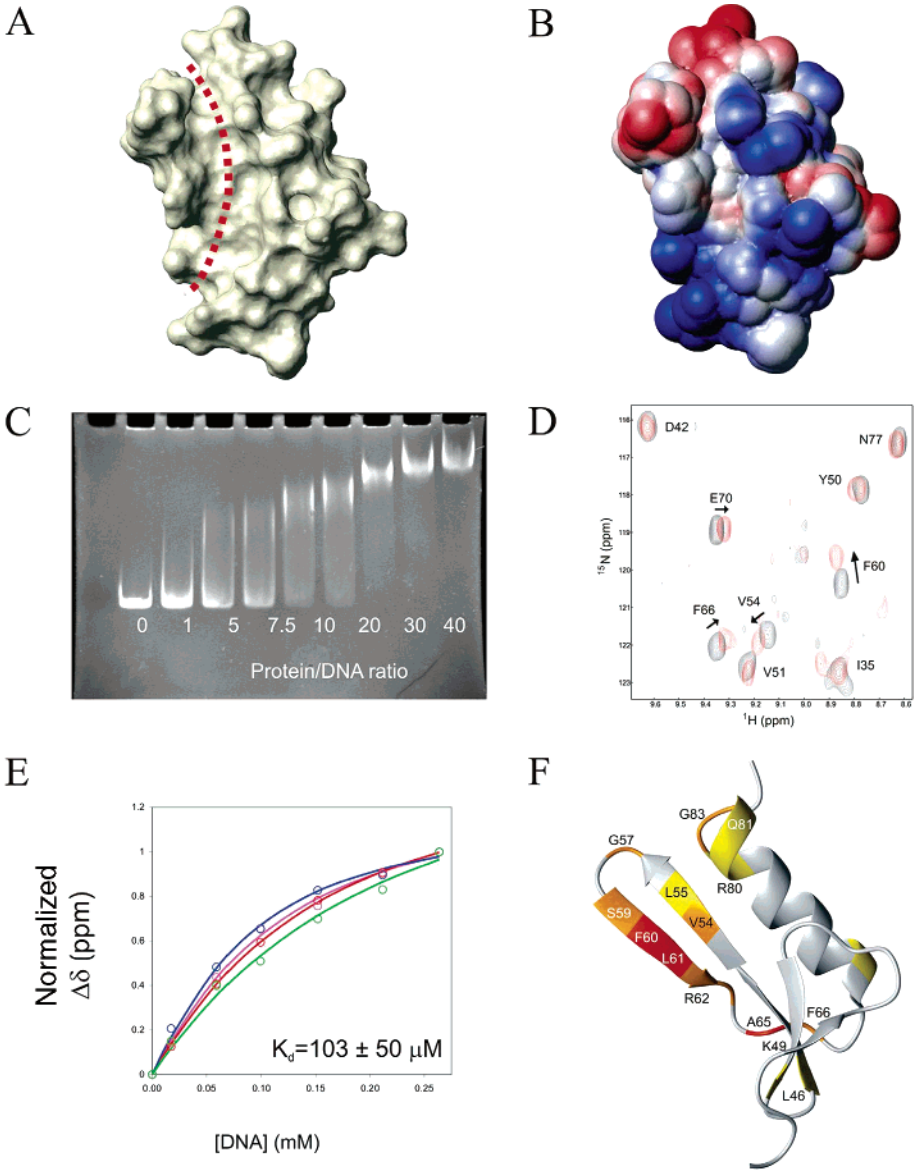

FIGURE 5: dsDNA binding properties of CedA. (A) Contact surface representation of CedA showing the potential binding surface. The red dashed line represents a groove on the DNA-binding surface. (B) Solvent accessible surface representation of CedA with the electrostatic potential in the same orientation as panel A. Red and blue colors indicate negative and positive charge, respectively. (C) DNA binding gel shift assay. (D) Region of the $^{1}H-^{15}N$ HSQC spectrum of CedA showing selected amide shift changes in the absence (black) and presence (red) of GCCGTTAACGCG. (E) Representative binding isotherms determined from fitting the change in NMR chemical shift to ligand concentration of a number of CedA amide peaks (chemical shift deviations are normalized). (F) Ribbon representation trace of CedA with residues experiencing DNA-induced chemical shift perturbations (red for large, orange for medium, and yellow for small). Panel F is in the same orientation as panel A.

major groove of dsDNA as seen in MDB1. The DNA-induced perturbations of the chemical shifts on the C-terminus of the helix probably arise from the secondary effects of the interaction of DNA with the β34 loop. It is also interesting to note that the N-terminal region of λ-INT-DBD is important for binding of DNA (*24*), suggesting that the N-terminus in CedA may also play an indirect role. Chemical shift perturbations are indeed observed in residues in the unstructured N-terminus of CedA, indicating that they may participate in an analogous fashion as seen in λ-INT-DBD. This stretch could form a structured element when bound to DNA, or loop along the groove as seen for the termini of Hin recombinase (*34*).

A prominent groove is present on the putative binding surface (Figure 5A) which is rich in aromatic residues, with Trp44, Phe53, and Phe60 forming the walls and floor of part of the groove. In MBD1 and MeCP2, hydrophobic pockets may bind the methyl groups of methylated DNA (*32*, *33*), and the aromatic residues, especially phenylalanines, may be used to provide ring stacking interaction in DNA and RNA (*29*, *35*) and intercalate between step bases (*36*).

In conclusion, CedA adopts a $\beta\beta\beta\beta\alpha$ topology reminiscent of dsDNA-binding domains from AtERF1 from *A. thaliana* and λ-integrase protein (λ-INT-DBD) from bacteriophage λ. A positive charge surface with exposed aromatic residues together with the mobile β34 loop is clearly implicated in dsDNA recognition. Further work is required to characterize the specific sequences that CedA binds and ultimately the role in CedA-induced cell division. The work presented in this paper provides an important framework upon which to build.

REFERENCES

1. Errington, J., Daniel, R. A., and Scheffers, D. J. (2003) Cytokinesis in bacteria, *Microbiol. Mol. Biol. Rev. 67*, 52.
2. Margolin, W. (2000) Themes and variations in prokaryotic cell division, *FEMS Microbiol. Rev. 24*, 531−548.
3. Romberg, L., and Levin, P. A. (2003) Assembly dynamics of the bacterial cell division protein FtsZ: Poised at the edge of stability, *Annu. Rev. Microbiol. 57*, 125−154.
4. Sherratt, D. J. (2003) Bacterial chromosome dynamics, *Science 301*, 780−785.
5. Messer, W. (2002) The bacterial replication initiator DnaA. DnaA and oriC, the bacterial mode to initiate DNA replication, *FEMS Microbiol. Rev. 26*, 355−374.
6. Katayama, T. (2001) Feedback controls restrain the initiation of *Escherichia coli* chromosomal replication, *Mol. Microbiol. 41*, 9−17.
7. Simmons, L. A., and Kaguni, J. M. (2003) The dnaAcos allele of *Escherichia coli*: Hyperactive initiation is caused by substitution of A184V and Y271H, resulting in defective ATP binding and aberrant DNA replication control, *Mol. Microbiol. 47*, 755−765.
8. Katayama, T., and Kornberg, A. (1994) Hyperactive Initiation of Chromosomal Replication in-Vivo and in-Vitro by a Mutant Initiator Protein, Dnaacos, of *Escherichia coli*, *J. Biol. Chem. 269*, 12698−12703.
9. Katayama, T., Takata, M., and Sekimizu, K. (1997) CedA is a novel *Escherichia coli* protein that activates the cell division inhibited by chromosomal DNA over-replication, *Mol. Microbiol. 26*, 687−697.
10. Wishart, D. S., Bigam, C. G., Yao, J., Abildgaard, F., Dyson, H. J., Oldfield, E., Markley, J. L., and Sykes, B. D. (1995) H-1, C-13 and N-15 Chemical-Shift Referencing in Biomolecular Nmr, *J. Biomol. NMR 6*, 135−140.
11. Bax, A. (1994) Multidimensional Nuclear-Magnetic-Resonance Methods for Protein Studies, *Curr. Opin. Struct. Biol. 4*, 738−744.
12. Bax, A., Clore, G. M., and Gronenborn, A. M. (1990) H-1-H-1 Correlation Via Isotropic Mixing of C-13 Magnetization, a New 3-Dimensional Approach for Assigning H-1 and C-13 Spectra of C-13-Enriched Proteins, *J. Magn. Reson. 88*, 425−431.
13. Yamazaki, T., Formankay, J. D., and Kay, L. E. (1993) 2-Dimensional NMR Experiments for Correlating C-13-β and H-1-δ/ϵ Chemical-Shifts of Aromatic Residues in C-13-Labeled Proteins Via Scalar Couplings, *J. Am. Chem. Soc. 115*, 11054−11055.
14. Delaglio, F., Grzesiek, S., Vuister, G. W., Zhu, G., Pfeifer, J., and Bax, A. (1995) Nmrpipe: A Multidimensional Spectral Processing System Based on Unix Pipes, *J. Biomol. NMR 6*, 277−293.
15. Bartels, C., Xia, T. H., Billeter, M., Guntert, P., and Wuthrich, K. (1995) The Program Xeasy for Computer-Supported NMR Spectral-Analysis of Biological Macromolecules, *J. Biomol. NMR 6*, 1−10.
16. Linge, J. P., Habeck, M., Rieping, W., and Nilges, M. (2003) ARIA: Automated NOE assignment and NMR structure calculation, *Bioinformatics 19*, 315−316.
17. Cornilescu, G., Delaglio, F., and Bax, A. (1999) Protein backbone angle restraints from searching a database for chemical shift and sequence homology, *J. Biomol. NMR 13*, 289−302.
18. Kay, L. E., Torchia, D. A., and Bax, A. (1989) Backbone Dynamics of Proteins as Studied by N-15 Inverse Detected Heteronuclear Nmr-Spectroscopy: Application to Staphylococcal Nuclease, *Biochemistry 28*, 8972−8979.
19. Farrow, N. A., Muhandiram, R., Singer, A. U., Pascal, S. M., Kay, C. M., Gish, G., Shoelson, S. E., Pawson, T., Formankay, J. D., and Kay, L. E. (1994) Backbone Dynamics of a Free and a Phosphopeptide-Complexed Src Homology-2 Domain Studied by N-15 NMR Relaxation, *Biochemistry 33*, 5984−6003.
20. Williamson, R. A., Carr, M. D., Frenkiel, T. A., Feeney, J., and Freedman, R. B. (1997) Mapping the binding site for matrix metalloproteinase on the N-terminal domain of the tissue inhibitor of metalloproteinases-2 by NMR chemical shift perturbation, *Biochemistry 36*, 13882−13889.
21. Wishart, D. S., Sykes, B. D., and Richards, F. M. (1991) Relationship between nuclear-magnetic-resonance chemical-shift and protein secondary structure, *J. Mol. Biol. 222*, 311−333.
22. Holm, L., and Sander, C. (1993) Protein-Structure Comparison by Alignment of Distance Matrices, *J. Mol. Biol. 233*, 123−138.
23. Allen, M. D., Yamasaki, K., Ohme-Takagi, M., Tateno, M., and Suzuki, M. (1998) A novel mode of DNA recognition by a β-sheet revealed by the solution structure of the GCC-box binding domain in complex with DNA, *EMBO J. 17*, 5484−5496.
24. Wojciak, J. M., Sarkar, S., Landy, A., and Clubb, R. T. (2002) Arm-site binding by λ-integrase: Solution structure and functional characterization of its amino-terminal domain, *Proc. Natl. Acad. Sci. U.S.A. 99*, 3434−3439.
25. Connolly, K. M., Wojciak, J. M., and Clubb, R. T. (1998) Site-specific DNA binding using a variation of the double stranded RNA binding motif, *Nat. Struct. Biol. 5*, 546−550.
26. Richardson, J. S., and Richardson, D. C. (2002) Natural β-sheet proteins use negative design to avoid edge-to-edge aggregation, *Proc. Natl. Acad. Sci. U.S.A. 99*, 2754−2759.
27. Connolly, K. M., Ilangovan, U., Wojciak, J. M., Iwahara, M., and Clubb, R. T. (2000) Major groove recognition by three-stranded β-sheets: Affinity determinants and conserved structural features, *J. Mol. Biol. 300*, 841−856.
28. Luscombe, N. M., and Thornton, J. M. (2002) Protein-DNA interactions: Amino acid conservation and the effects of mutations on binding specificity, *J. Mol. Biol. 320*, 991−1009.
29. Kim, Y. C., Geiger, J. H., Hahn, S., and Sigler, P. B. (1993) Crystal-Structure of a Yeast Tbp TATA-Box Complex, *Nature 365*, 512−520.
30. Somers, W. S., and Phillips, S. E. V. (1992) Crystal-Structure of the Met Repressor-Operator Complex at 2.8 Å Resolution Reveals DNA Recognition by β-Strands, *Nature 359*, 387−393.
31. Cohen, S. X., Moulin, M., Hashemolhosseini, S., Kilian, K., Wegner, M., and Muller, C. W. (2003) Structure of the GCM domain-DNA complex: A DNA-binding domain with a novel fold and mode of target site recognition, *EMBO J. 22*, 1835−1845.
32. Ohki, I., Shimotake, N., Fujita, N., Jee, J. G., Ikegami, T., Nakao, M., and Shirakawa, M. (2001) Solution structure of the methyl-CpG binding domain of human MBD1 in complex with methylated DNA, *Cell 105*, 487−497.
33. Wakefield, R. I. D., Smith, B. O., Nan, X. S., Free, A., Soteriou, A., Uhrin, D., Bird, A. P., and Barlow, P. N. (1999) The solution structure of the domain from MeCP2 that binds to methylated DNA, *J. Mol. Biol. 291*, 1055−1065.
34. Feng, J. A., Johnson, R. C., and Dickerson, R. E. (1994) Hin Recombinase Bound to DNA: The Origin of Specificity in Major and Minor-Groove Interactions, *Science 263*, 348−355.
35. Simpson, P. J., Monie, T. P., Szendroi, A., Davydova, N., Tyzack, J. K., Conte, M. R., Read, C. M., Cary, P. D., Svergun, D. I., Konarev, P. V., Curry, S., and Matthews, S. (2004) Structure and RNA interactions of the N-terminal RRM domains of PTB, *Structure 12*, 1631−1643.
36. Rice, P. A., Yang, S. W., Mizuuchi, K., and Nash, H. A. (1996) Crystal structure of an IHF-DNA complex: A protein-induced DNA u-turn, *Cell 87*, 1295−1306.
37. Laskowski, R. A., Rullmann, J. A. C., MacArthur, M. W., Kaptein, R., and Thornton, J. M. (1996) AQUA and PROCHECK-NMR: Programs for checking the quality of protein structures solved by NMR, *J. Biomol. NMR 8*, 477−486.

BI0500269